The Thermal State of the Intergalactic Medium at Redshift $5 < z < 6$

Jiren Liu and Li-Zhi Fang[1]

ABSTRACT

The thermal state of the intergalactic medium (IGM) at high redshift is crucial to understand the physics of reionization, as the temperature and its evolution are closely related to reionization process. We develop a method to measure the temperature of the IGM at $5 < z < 6$ with Lyα absorption spectra of quasars. Using hydrodynamic simulation samples of the ΛCDM cosmology, we show that the probability distribution function (PDF) of the transmission fluxes and the profile of Lyα leaks are sensitive to the thermal state of the IGM; higher temperature yields lower peak, narrower broadening, and smoother profile. This is mainly due to the thermal broadening of Lyα absorption around low mass density voids. We found the width function $n(W, z)$, defined as the number of leaks of width W at redshift z per unit W per unit z, is an effective tool to constrain the temperature of the IGM. We fit the $n(W, z)$ of seven high-resolution spectra of quasars at $z \simeq 6$ with simulation samples of different thermal states. The main results are: 1. the temperature at the mean density, T_0, is most likely larger than 1.3×10^4 K at $5 < z < 6$; 2. T_0 shows no evolution from redshift $z = 5$ to 6.

Subject headings: cosmology: theory - intergalactic medium - large-scale structure of the universe

[1]Department of Physics, University of Arizona, Tucson, AZ 85721

1. Introduction

The physical states of the IGM at redshift $z > 5$ are crucial to understand the history of structure evolution, as they are directly related to the formation and evolution of early luminous objects. Three kinds of physical properties of the IGM are important: ionization state, chemical abundance, and thermal state. The UV radiation of first generation of luminous objects will reionize the neutral IGM; current observation of the absorption spectra of distant quasars and the polarization of CMB photons indicate an extended reionization epoch (e.g., Fan et al. 2006; Spergel et al. 2007). The metal abundance of the IGM reflects the chemical feedback of early galaxies and the properties of early stars (Qian & Wasserburg 2005), and metal absorption lines on several quasars at $z > 5$ are analyzed (Songaila 2005; Becker et al. 2006). The thermal state of the IGM is closely related to the reionization process, however, no detection or constraint on the temperature of the IGM at redshift $z > 5$ is reported yet.

When the IGM is reionized by the UV radiation of first generation of luminous objects, it is also heated up to tens thousand degrees which depends on the ionizing spectrum and radiation transfer effect (Abel & Haehnelt 1999). Subsequently, the evolution of the temperature of the IGM is mainly determined by the expansion of the universe and the photoionization heating of the remaining neutral ions. Thus, the observed temperature can be used to constrain the history of reionization (Miralda-Escude & Rees 1994; Haehnelt & Steinmetz 1998; Theuns et al. 2002; Hui & Haiman 2003). Moreover, the temperature is also important for estimating the photoionization rate required to maintain the ionization equilibrium, because the recombination rate depends sensitively on temperature.

The temperature of the IGM at redshift $z < 5$ can be measured with the width of Lyα absorption lines, which is determined by thermal broadening and velocity field (Schaye et al. 1999), or by parameter fitting to the cutoff of the Lyα forest power spectrum (Zaldarriaga et al. 2001). Because the opacity of the IGM increases rapidly at high redshift, the spectra of quasars at $z > 5$ do not show forest features any more, but consist of complete Gunn-Peterson absorption troughs separated by tiny flux spikes. As a result, it is no longer possible to measure the temperature of the IGM at redshift $z > 5$ through the absorption line width. New statistics sensitive to temperature are needed.

In this paper, we propose a method effective to measure the temperature of the IGM at redshift $5 < z < 6$. It is based on Lyα leaks, which are defined to be the emissive regions in complementary to otherwise zero-flux absorption gaps in the absorption spectra of high redshift quasars. Similar to identifying individual absorption lines at low redshift, we can decompose the spectra at $z > 5$ into isolated Lyα leaks. Their profiles can be described by the equivalent width (EW) and the width scale (W), which reflect the strength of leaking

and the scale of leaking regions, respectively (Liu et al. 2007; Feng et al. 2008).

The observed statistical features of Lyα leaks at $z < 6$ can be well fitted with hydrodynamic simulations in the ΛCDM cosmology assuming the ionizing background to be uniform. It revealed that the majority of Lyα leaks at $z < 6$ are from low mass density voids (Liu et al. 2007). That is, the Lyα leaks at $z < 6$ are actually manifestations of low mass density voids, which are less affected by shock heating and contain a pure thermal memory due to reionization. We will show that the width of Lyα leak profile is very sensitive to the thermal state of the IGM and provides an effective tool to probe the thermal history of the IGM at redshift $5 < z < 6$.

This paper is arranged as follows. The observed data and simulation samples are given in §2. §3 and §4 show how the thermal state affects Lyα leaks and present the comparison between observed and simulated samples. It shows that the distribution of the width of Lyα leaks is very sensitive to the IGM temperature. §5 describes the method and results of temperature measurement (fitting) at $5 < z < 6$. Possible systematics and implications of the results are discussed in §6.

2. Samples

2.1. Observational data

The thermal effect is apparent only when the resolution of observational spectra is comparable or higher than the scale of typical thermal velocity of the IGM ($\sim$ tens km/s). Therefore, we use 7 high-resolution ($\sim$ 7 km/s) spectra of quasars at $z \geq 5.8$ taken by High Resolution Echelle Spectrometer (HIRES) of Keck I (Becker et al. 2007). The most challenging problem of data reduction at redshift $z \simeq 6$ is the subtraction of sky background and sky emission lines, because the fluxes on the blueside of Lyα emission lines are almost fully absorbed, and the signal level is very low. To handle this difficulty, we modify the MAKEE package, written by Tom Barlow, to include a 2D sky model of Kelson (2003).

To avoid the mixing of Lyβ absorption and the effect of quasar's H II region, only the rest frame wavelength between 1050 to 1170 Å are used. To study the redshift evolution of the temperature, we divide the spectra into three redshift bins: $5.1 < z < 5.4$, $5.4 < z < 5.7$, and $5.7 < z < 6.0$. The observational data are, respectively, rebinned in wavelength to 0.63, 0.68, and 0.73 Å at above three redshift bins, which match the corresponding numerical resolution of simulation (see §2.2). The observed flux, f_{obs}, is normalized with a power-law continuum $f_{con} \propto \nu^{-0.5}$. The effect of continuum fitting will be discussed in §6.1.

2.2. Simulation samples

We produce simulation samples with the hybrid hydrodynamic N-body code based on Weighted Essentially Non-oscillatory (WENO) scheme (Feng et al. 2004). It is in Eulerian scheme and suitable to study the fluid in high as well as in low mass density areas. The WENO samples have been successfully applied to reveal the self-similar hierarchy behavior of cosmic baryon fluid (Kim et al. 2005; He et al. 2006; Liu & Fang 2008), to explain the H I and He II Lyα absorption in quasar spectra (Liu et al. 2006b), and to study the relation between X-ray luminosity and temperature of groups of galaxies (Zhang et al. 2006). It is also used for studying Lyα leaks (Liu et al. 2007).

The simulation is performed in a comoving cubic box of 100 h^{-1} Mpc with a 512^3 grid and an equal number of dark matter particles. The grid size is $100/512 \sim 0.2$ h^{-1} Mpc. It is enough to catch the thermal effect when the temperature is equal to or larger than 10^4 K. We use the concordance ΛCDM cosmology model with parameters $\Omega_{\rm m}$=0.27, $\Omega_{\rm b}$=0.044, Ω_Λ=0.73, h=0.71, σ_8=0.84, and spectral index $n = 1$. The transfer function is calculated using CMBFAST (Seljak & Zaldarriaga 1996). We take a primordial composition of H and He (X=0.76, Y=0.24). The ionization fraction is calculated with ionization-recombination equilibrium.

According to the commonly accepted scenario of reionization, at early stages, only isolated patches around ionizing sources are highly ionized. The subsequent growing and overlapping of ionizing patches lead to a uniform ionizing background and the end of reionization (e.g., Ciardi et al. 2003; Sokasian et al. 2003; Gnedin 2004; Mellema et al. 2006). The ionization fraction of the IGM and the ionizing radiation undergo an evolution from highly non-uniform patches to an homogeneous field. Therefore, before the patch-to-uniform transition, the temperature field of the IGM is highly inhomogeneous; in this stage, it would be worthless to define a mean temperature of the IGM. If the patch-to-uniform transition happens rapidly enough, the thermal growth can be treated as a a sudden boost of temperature.

On the other hand, at lower redshift $z < 2$, the IGM is significantly heated by the shock heating due to structure formation (Cen & Ostriker 1999). It leads to a multiphase temperature-density relation (e.g., He et al. 2004). Since the thermal energy given by shock heating generally is larger than the initial thermal energy, the temperature of the IGM at $z < 2$ is almost independent of the initial thermal state. That is, the information of the IGM temperature at high redshift is washed out at $z < 2$.

The evolution of the IGM is relatively simple after the establishment of a uniform ionizing background and before the shock heating becomes strong. In this epoch, the temperature of low density regions is mainly determined by the expansion of the universe and the pho-

toionization heating of the remaining neutral ions, and the IGM still contains the memory of early thermal history. The temperature-density relation for low densities can be well approximated by a polytropical relation, $T = T_0(\rho/\bar{\rho})^{\gamma-1}$, here T_0 is the temperature at the mean density $\bar{\rho}$, and γ is the index of the "equation of state" (Hui & Gnedin, 1997).

We argue that the redshift range $5 < z < 6$ is in this "simple evolution" epoch. First, at $z \simeq 6$, a uniform ionizing background is well consistent with the probability distribution function (PDF) of the transmission flux, the evolution of dark gaps (Liu et al. 2006a), and the distribution of the equivalent width of Lyα leaks (Liu et al. 2007). It strongly suggests that the patch-to-uniform transition takes place at redshift $z > 6$. Second, hydrodynamic simulations show that the shock heating is unimportant at $z \simeq 6$ for low density areas compared with the thermal input of reionization. In this paper we assume a uniform ionizing background and study the thermal state of the IGM at $5 < z < 6$.

Generally speaking, to study different thermal histories, we should run a set of simulations with different thermal input at different redshift. Since the Lyα leaks are from low density voids and the polytropical relation works well for such densities, to speed up the calculation and study a large parameter space, we estimate the temperature field of the IGM through the polytropical relation. That is, we only run one simulation to get the density and velocity fields with an input of thermal energy of 2×10^4 K at $z = 10$ to mimic the thermal boost due to reionization. Then, the temperature field at $5 < z < 6$ are calculated using $T = T_0(\rho/\bar{\rho})^{\gamma-1}$ with different T_0 and γ. For given T_0 and γ, the photoionization rate is not free, but adjusted to fit the observed opacity at corresponding redshift.

This method implicitly assumes that the the density distribution of baryon fluid is independent of the initial condition of thermal state. This assumption is reasonable for baryon fluid at high redshift and low densities. The dynamical effect of initial thermal state is due to the pressure of the fluid. However, the sound speed at $T_0 \sim 10^4$ K is only a few km s^{-1}, and its effect is negligible if we consider only the mass field on comoving scales larger than 0.2 h^{-1} Mpc at redshift $z \simeq 6$.

3. Temperature dependence of transmission flux

3.1. The temperature effect on absorption spectrum

At redshift $z < 5$, the measurement of temperature is based on the width of absorption line profiles, which are determined by thermal broadening and velocity field (Schaye et al. 1999). Due to the increases of opacity at high redshift, the absorption lines become complete absorption troughs, and only a few big leaks dominate the total flux. The method based on

Lyα absorption lines does not help anymore. However, we can still expect some imprints of thermal state on the absorption spectrum.

As an example, we simulate three spectra with $\gamma = 1.3$ and $T_0 = 1, 2$, and 4 $\times 10^4$ K at $z = 5.5$; the photoionization rates are, respectively, 0.63, 0.48, and 0.3 $\times 10^{-12}$s^{-1}, which give a same mean flux 0.057 for the three temperature cases. The baryon density, the neutral hydrogen fraction, and the transmission flux are shown in Figure 1.

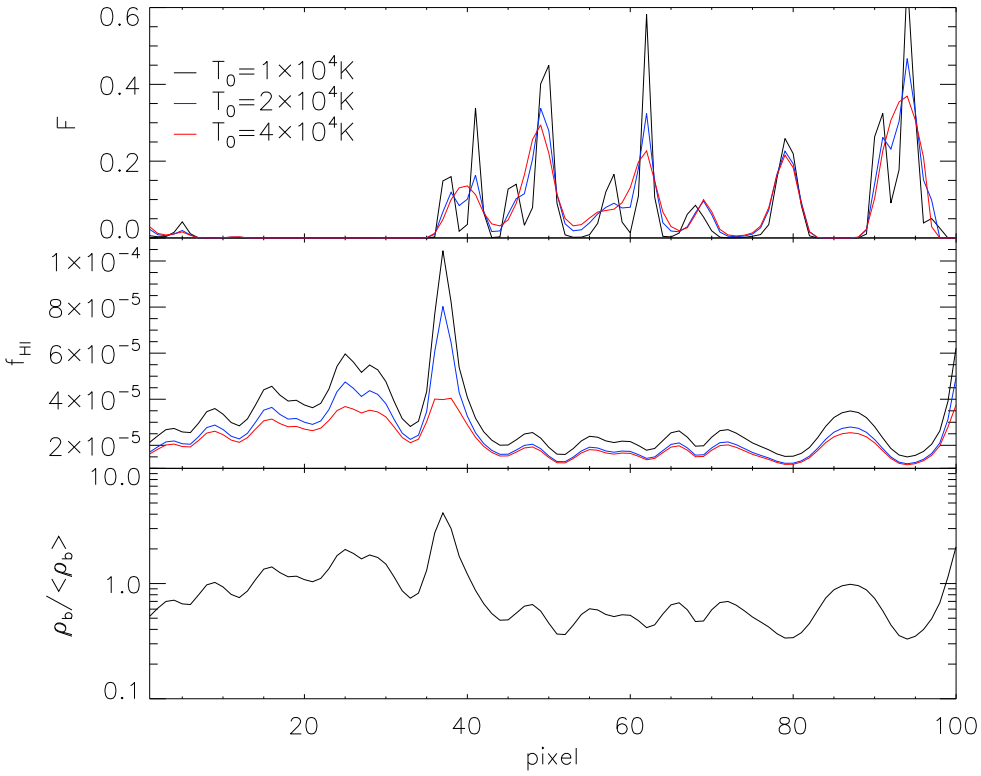

Fig. 1.— A simulation example of the baryon density field ρ_b (bottom panel), the neutral hydrogen fraction $f_{\rm HI}$ (middle panel) and the transmission flux F (top panel). The photoionization rate is adjusted to give a same opacity for T_0 =1 (black), 2 (blue), and 4 (red) $\times 10^4$ K. To give a same opacity, the neutral hydrogen fraction is different for different temperature; the distribution of resulting transmission flux is also different for different temperature.

The middle panel of Figure 1 shows that to fit a given Gunn-Peterson opacity, as that given by the observed value, different temperature of the IGM requires different fraction of neutral hydrogen. The higher the temperature T_0, the lower the fraction. While the neutral hydrogen fraction is determined by the balance between photoionization and recombination, the absorption optical depth is given by a Voigt function convolution of the neutral hydrogen

field. Consequently, for higher temperature, the absorption optical depth around a void is given by a larger region, and the neutral hydrogen fraction is smaller in order to produce the same opacity. This behavior is very different from the result neglecting thermal broadening effect, for which a given neutral hydrogen distribution corresponds to only one opacity (see, e.g. Songaila & Cowie 2002).

The top panel of Figure 1 shows that the profiles of Lyα leaks (flux spikes) depend sensitively on T_0 in spite of that they have the same mean flux. In general, leaks have lower peak, broader width, and smoother profile for higher T_0. These features are from the same reason as mentioned above. Thus, we can set constraints on the thermal state of the IGM by comparing the observed Lyα leaks with simulation samples, which have the same mean flux as the observation, but are of different thermal states.

3.2. PDF of transmission flux

Figure 1 shows that the transmission fluxes contain higher peaks for lower temperature T_0, which implies that the PDF of flux F will show a longer tail for lower T_0. Figure 2 presents the PDF of simulated flux for samples with $T_0 = 1$, 1.9, and 3.1×10^4 K and $\gamma = 1.2$, 1.4, and 1.6 at three redshift bins $z = 5.1$–5.4, 5.4–5.7, and 5.7–6.0. We see that in all cases the flux PDF of $T_0 = 1 \times 10^4$ K shows much longer tail than that of $T_0 = 1.9 \times 10^4$ and 3.1×10^4 K. On the other hand, the difference of the PDF between $T_0 = 1.9 \times 10^4$ and 3.1×10^4 K is small. That is, the PDF of flux is more sensitive to low temperatures of $T_0 \leq 2 \times 10^4$ K. The PDF also shows a weak dependence on parameter γ.

We also present the PDF of the 7 quasars observed by HIRES in Figure 2, for which the error bars are given by Poisson fluctuations. The observed PDF strongly supports $T_0 > 1 \times 10^4$ K for all γ at all three redshift bins. While the observed PDF is consistent with simulation of $T_0 > 1.9 \times 10^4$ K at $z < 5.7$, it shows some discrepancy with simulation at $z > 5.7$. This should be due to noise contamination, which is more serious at $z > 5.7$, and the observational spectra have more pixels with $F < 0.1$ than simulation samples.

4. Temperature dependence of the profile of Lyα leaks

As shown in Figure 1, for a same opacity, the profile of Lyα leaks is different for different temperature and is useful to constrain the temperature of the IGM. We need a method to pick up Lyα leaks and some quantities to characterize their profiles. Similar to Liu et al. (2007), Lyα leaks are identified as contiguous regions where the fluxes are larger than a

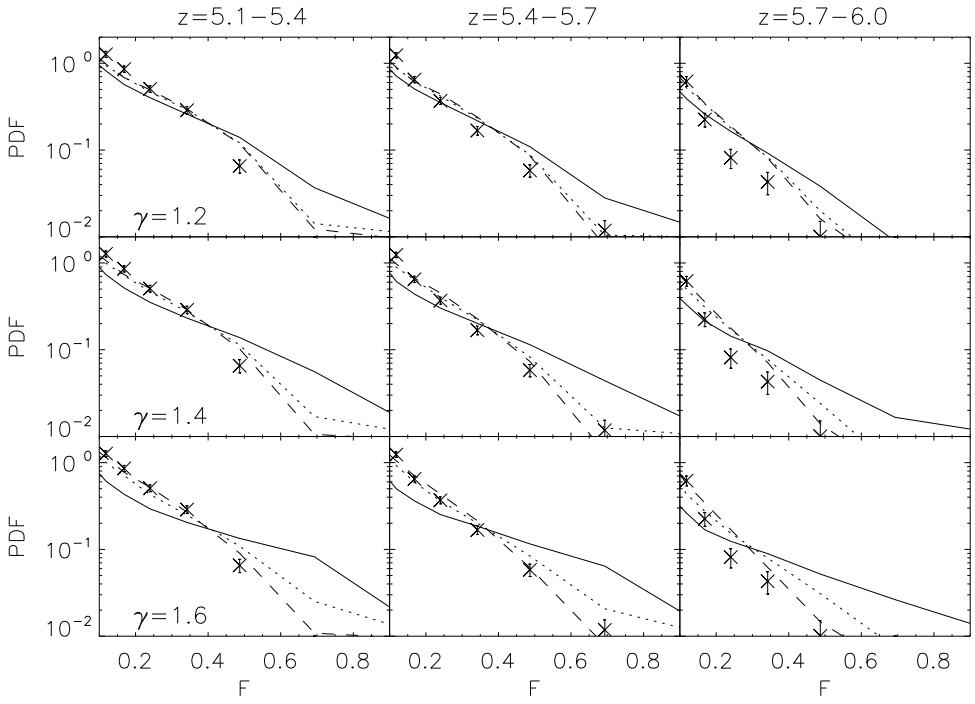

Fig. 2.— PDF of the simulated flux with T_0=1 × 10^4 K (solid lines), 1.9 × 10^4 K (dotted lines), and 3.1 × 10^4 K (dashed lines), and γ=1.2 (top), 1.4 (middle), and 1.6 (bottom) at redshift bins z = 5.1–5.4, 5.4–5.7, and 5.7–6.0. The observational data of 7 quasars are also shown, for which the error bars are from Poisson errors. The temperature of $T_0 = 1 \times 10^4$ is impossible to fit the observed PDF.

given threshold F_{th}. If there are two local maximums, each one is identified as a leak. The boundaries of a leak are positions where the fluxes are smaller than F_{th}, or the minimum between two neighboring maxima. We take the threshold $F_{th} = 0.06$, which corresponds to about 2 σ of the observational noise. The effect of changing F_{th} will be discussed in §6.2.

Similar to emission and absorption lines, we can define the equivalent width of a leak as the area under its flux profile, $EW = \int F d\lambda$, where the integral is over the range between its boundaries. We also define the width of a leak W as the distance between its boundaries. Intuitively, EW measures the strength of leaking, or the Gunn-Peterson optical depth within leaking regions, and W reflects the spatial scale of leaking regions.

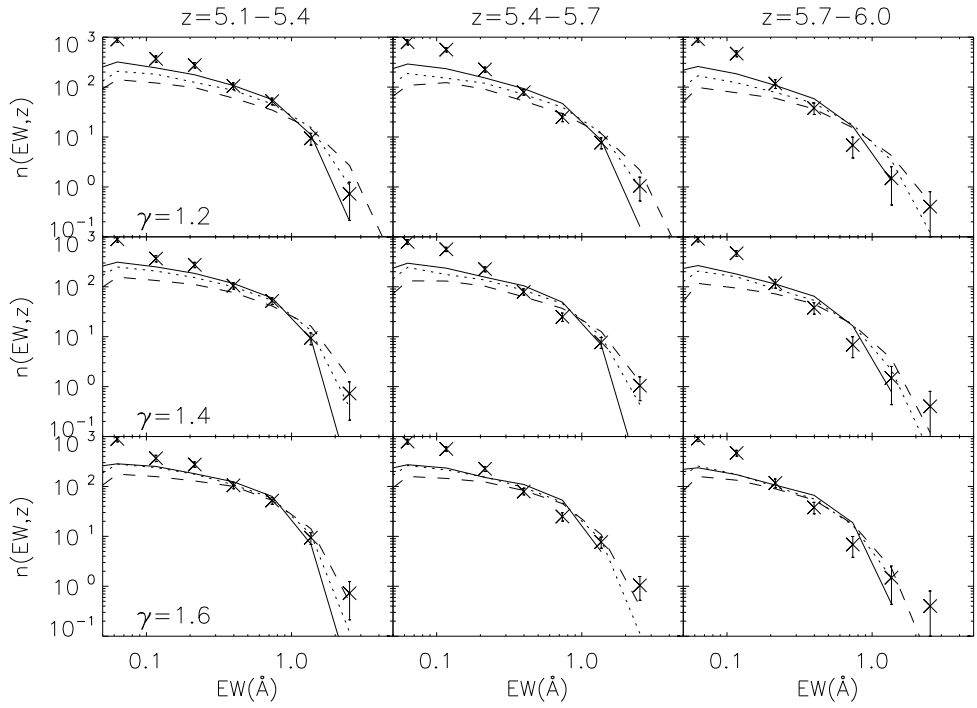

Fig. 3.— Equivalent width function $n(EW, z)$ of the simulated samples with T_0=1 × 10^4 K (solid lines), 1.9 × 10^4 K (dotted lines), and 3.1 × 10^4 K (dashed lines), and γ=1.2 (top), 1.4 (middle), and 1.6 (bottom) at redshift bins z = 5.1–5.4, 5.4–5.7, and 5.7–6.0. The observational data of 7 quasars are also shown, for which the error bars are from Poisson errors. The observed leaks at $EW < 0.2$ Å are heavily affected by noise. Because the requirement of the same opacity, $n(EW, z)$ of different thermal states are similar.

4.1. Distribution of equivalent width *EW*

The first statistic we used is the equivalent width function $n(EW, z)$, which is the number of leaks of EW at redshift z per unit EW per unit z. $n(EW, z)$ reflects the distribution of the strength of leaking and is generally different for uniform ionizing background and fluctuating background (Liu et al. 2007; Feng et al. 2008).

Figure 3 plots $n(EW, z)$ for simulation samples of T_0 = 1, 1.9, and 3.1×10^4 K and γ=1.2, 1.4, and 1.6 at three redshift bins z = 5.1–5.4, 5.4–5.7, and 5.7–6.0. The distributions of $n(EW, z)$ depend weakly on parameters T_0 and γ. The reason can be seen from Figure 1. The leaks of lower temperature generally show higher peak and narrower broadening, while

the leaks of higher temperature have lower peak and wider broadening, and therefore, the areas of Lyα leaks of different thermal states are actually similar. This result essentially comes from the requirement that samples of different thermal states have the same opacity.

We also plot $n(EW, z)$ for leaks of the 7 observed quasars in Figure 3, and the error bars are from Poisson fluctuations. The observed distributions of $n(EW, z)$ are basically consistent with simulation results. For leaks of $EW < 0.2$ Å, the observed number is a little higher than simulated value. This is due to the contamination of observational noise. That is, many leaks with small EW actually are due to noise. As has been shown in Liu et al. (2007), if we add the noise of observational noise level to the simulation samples, they will yield similar $n(EW, z)$ at small EW as observed samples.

4.2. Distribution of width W

Similar to $n(EW, z)$, we define the width function $n(W, z)$ as the number of leaks of W at redshift z per unit W per unit z. As showed in Feng et al. (2008), W does not correlate with EW and is an independent measurement of the profile of Lyα leaks. Figure 1 shows that the width of Lyα leaks is very sensitive to T_0. We study the distribution of W in detail now.

Figure 4 presents $n(W, z)$ for simulation samples of $T_0 = 1$, 1.9, and 3.1×10^4 K and $\gamma = 1.2$, 1.4, and 1.6 at three redshift bins $z = 5.1$–5.4, 5.4–5.7, and 5.7–6.0. We see that the distributions of $n(W, z)$ are substantially dependent on T_0. At $W = 6$ Å, $n(W, z)$ of $T_0 = 1 \times 10^4$ and 3.1×10^4 K have a difference of a factor of 30 for all γ and redshifts.

Generally speaking, samples with lower T_0 lack wider leaks, and the tail of $n(W, z)$ at large W is much lower than high T_0 samples. Higher γ yields a lower temperature at density voids of $\rho < \bar{\rho}$ and also gives a shorter tail of $n(W, z)$ at large W. Samples at lower redshift contain more large leaks, and the tail of $n(W, z)$ is also longer than higher redshifts.

The width function $n(W, z)$ of the 7 observed quasars is also plotted in Figure 4, for which the error bars are from Poisson fluctuations. Similar to Figure 2, for all γ and redshift bins, the observed $n(W, z)$ can not fit with simulation samples of $T_0 = 1 \times 10^4$ K. On the other hand, for $\gamma = 1.2$, samples of $T_0 = 1.9 \times 10^4$ K gives better fitting to observational data, while for $\gamma = 1.6$, samples of $T_0 = 3.1 \times 10^4$ K is better. That is, the width function $n(W, z)$ of Lyα leaks is sensitive to both T_0 and γ and is effective to detect the thermal state of the IGM.

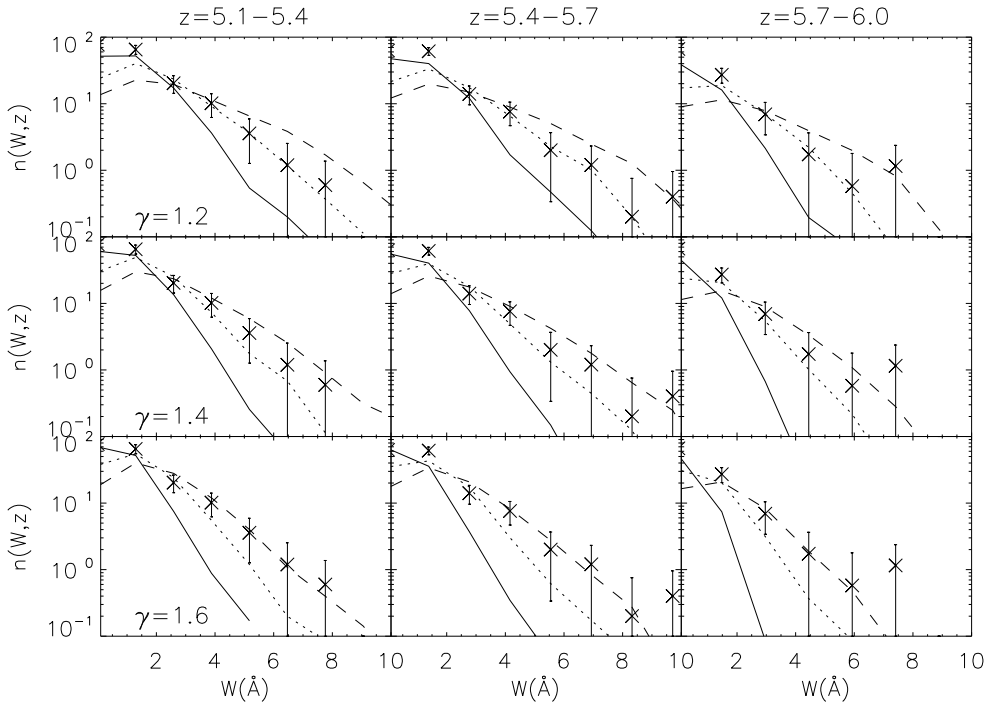

Fig. 4.— Width function $n(W, z)$ of the simulated leaks with T_0=1 × 10^4 K (solid lines), 1.9 × 10^4 K (dotted lines), and 3.1 × 10^4 K (dashed lines), and γ=1.2 (top), 1.4 (middle), and 1.6 (bottom) at redshift bins z = 5.1–5.4, 5.4–5.7, and 5.7–6.0. The observational data of 7 quasars are also shown, for which the error bars are from Poisson errors. $n(W, z)$ is very sensitive to different thermal state and can be used to constrain the thermal state of the IGM.

5. Fitting method and results

The PDF of the flux is insensitive to temperatures higher than 2 × 10^4 K. It is also insensitive to the parameter γ. The equivalent width function $n(EW, z)$ is almost independent of the temperature T_0. Therefore, we only use the width function $n(W, z)$ to constrain the thermal state of the IGM. The fitting method and results are given in next two sections.

5.1. Fitting method

First, we need to estimate the errors of the observed $n(W, z)$. The Gunn-Peterson optical depths along different lines of sight show large scatter at $z \simeq 6$ (Fan et al. 2006). Though the scatter might come from the fluctuations of ionizing background, the density fluctuation itself already provides enough scatter (Liu et al. 2006a; Lidz et al. 2006). We assume the variance of $n(W, z)$ come from the fluctuation of density field.

To estimate the variance of the observed $n(W, z)$ of 7 quasars, we use 100 simulation lines of flux with $\gamma = 1.3$ and $T_0 = 1.9 \times 10^4$ K. We divide the 100 samples into 14 subsets, each of which contains 7 lines, and calculate $n(W, z)$ for each subset. We then calculate the variance among the subsets. The result at $z = 5.4$–5.7 is shown in Figure 5. The Poisson errors are also shown in Figure 5, which are shifted slightly to right. It is clear from Figure 5 that the errors due to small sample size (total 7 samples available) are larger than Poisson fluctuations and dominate the error of the current measurement.

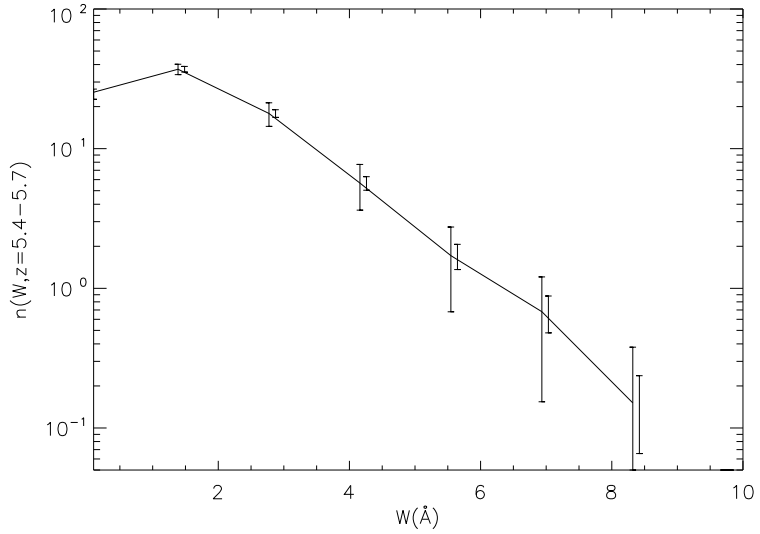

Fig. 5.— Variance of simulation samples of observational sample size for $n(W, z)$. The Poisson errors are also shown, which is shifted slightly to right. The measurement errors of $n(W, z)$ given by the 7 quasars are dominated by the small sample size.

We create a 2D grid of thermal state (T_0, γ) with the following values:

$$\begin{aligned} T_0 &= 1, 1.3, 1.6, 1.9, 2.2, 2.5, 2.8, 3.1 \times 10^4 \mathrm{K}; \\ \gamma &= 1, 1.1, 1.2, 1.3, 1.4, 1.5, 1.6. \end{aligned}$$

For each point in the (T_0, γ) plane we extract 100 lines randomly from the simulation samples and adjust the photoionization rate to match the mean flux as the observed values at the corresponding redshift. We use χ^2 as the merit function to fit the observed $n(W, z)$ with simulation samples of different thermal states. The χ^2 function is given by

$$\chi^2 = \sum_i \frac{(d_i - s_i)^2}{\sigma_i^2}, \tag{1}$$

where d_i is the observed $n(W, z)$, s_i is the simulated value, and σ_i is the variance calculated from simulation samples as mentioned above. Only three data points of $n(W, z)$ between 3 and 7 Å are used at all three redshift bins. This is because data points of $W > 7$ Å show strong dependence on binning, while data points of $W < 3$ Å are heavily affected by noise.

5.2. Results

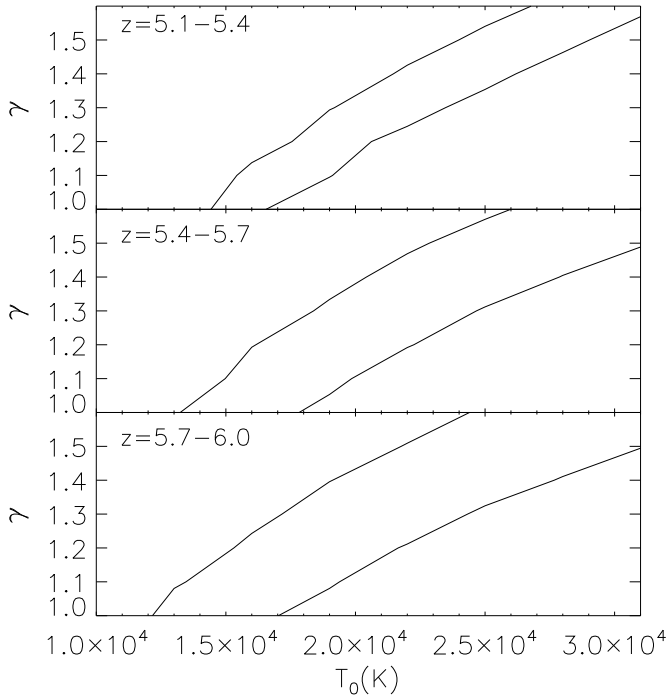

Fig. 6.— Constraints on the thermal state plane $T_0 - \gamma$ at redshift bins $z = 5.1$–5.4, 5.4–5.7, 5.7–6.0. The contour lines are of constant χ^2 with $\Delta\chi^2$=2.3, which corresponds to 68% of the area of a two-dimensional Gaussian.

The constraints in the parameter space (T_0, γ) are shown in Figure 6, in which the

contours are lines of constant χ^2 with $\Delta\chi^2$=2.3, which corresponds to 68% confidence of a two-dimensional Gaussian. Due to the large errors from the small size of observed samples, the allowed parameter space is still broad. Nevertheless, it already yields useful results. The most confident conclusion is that the temperature T_0 for all three redshift bins is larger than 1.3×10^4 K. This result is also supported by the PDF of the flux (Figure 3). On the other hand, the allowed parameter space shows little evolution from $z = 5.1$ to 6.0.

The 68% contour has an interesting behavior: the larger the γ, the larger the T_0. This is directly related to the fact that Lyα leaks are from low density voids. Considering the relation $T = T_0(\rho/\bar{\rho})^{\gamma-1}$, for $\rho < \bar{\rho}$, the effect on T given by an increase of T_0 will be canceled by an increase of γ. Therefore, the fitting with smaller T_0 and γ will be the same as larger T_0 and γ. Obviously, this feature will not be true in high densities of $\rho > \bar{\rho}$.

In fact, we can estimate the density of voids responsible for Lyα leaks with the slope of allowed band in the (T_0, γ) plane. The observed $n(W, z)$ requires a certain temperature at voids of some density. From relation $T = T_0(\rho/\bar{\rho})^{\gamma-1}$, we get $\ln(\rho/\bar{\rho}) = -d \ln T_0/d\gamma$. From Figure 6, $dT_0/d\gamma \simeq 1.2 \times 10^4/0.6$; adopting a $T_0 = 2 \times 10^4$ K, we get $\rho \simeq 0.4\bar{\rho}$. It is the typical density of voids yielding Lyα leaks.

6. Discussions and conclusion

6.1. Possible systematics

In this section we discuss possible systematics that can affect the results. We first assess the justice of the assumptions of our model.

First, to produce the temperature field, we use a polytropical temperature-density relation. It is reasonable for the low density voids, which are responsible for Lyα leaks. Second, we assume a uniform ionizing background, which should be applicable at least at redshift $z < 5.7$. Third, we use a fixed set of cosmological parameters of the ΛCDM model. Though cosmological parameters have been measured to a precision of about ten percent, some parameters still show discrepancies between different measurements (e.g., Spergel et al. 2007). Since Lyα leaks at $z > 6$ are due to low-density voids, parameters which determine the structure formation will affect the distribution of Lyα leaks. The most relevant parameter is σ_8, the amplitude of power spectrum of density fluctuation. We have run simulations of σ_8 =0.74 and 0.94. The distribution of EW is almost the same as the result of σ_8 =0.84. This is because σ_8 mainly affect the amplitude of the density fluctuation, and its effect is reduced by requiring that all samples should have the same mean flux. σ_8 does affect the distribution of the width W. Higher σ_8 predicts steeper void and narrower width. But the

difference is smaller than the variance caused by the sample size.

Since the scatter of optical depths among different line-of-sight is large, the small size of our samples might be biased relative to the real distribution. We randomly sample different number of lines and calculate $n(W, z)$ using our simulation samples. We found 25 random lines at $z = 5.4$–5.7 are needed to make $n(W, z)$ converge to the distribution of 100 lines. When more observational samples are available, we can get tighter limit and more fare estimation.

The errors from reduction process, like remaining sky emission lines and cosmic rays will affect the transmission flux and the fitted temperature. We estimate the uncertainties due to the continuum fitting by changing the continuum level with $\pm 10\%$ level, and find that the results are similar. We also tried different leak identification with F_{th}=0.08, which corresponds to different signal level. The results are also similar to the default F_{th}=0.06.

6.2. Implication of the results

Although the statistical confidence level is still poor, we already have two tentative conclusions: 1. a low temperature of $T_0 < 1.3 \times 10^4$ K at $5 < z < 6$ is disfavored; 2. the temperature T_0 shows no evolution from redshift $z = 5$ to 6. These two results already provide useful insights into the thermal evolution of the IGM.

If the mean temperature of the IGM $\simeq 2 \times 10^4$ K at $z \simeq 6$, the required photoionization rate of reionization, or star formation rate, is smaller by a factor of 2 in comparison with 1×10^4 K. Therefore, the first conclusion supports the argument that galaxies are sufficient for reionization at $z \simeq 6$ by Stiavelli et al. (2004), who assumed a temperature of 2×10^4 K.

We can set constraints on the reionization history with the thermal state of the IGM. If reionization occurs rapidly and the IGM remains highly ionized, the temperature of the IGM is determined by the balance between expansion cooling and photoionization heating and can be used to constrain the history of reionization (Miralda-Escude & Rees 1994; Haehnelt & Steinmetz 1998; Theuns et al. 2002; Hui & Haiman 2003). This model concludes that if reionization happened early enough, an asymptotic temperature of $T_0 < 1 \times 10^4$ K will be reached.

However, we find that the temperature shows little evolution from $z = 5.1$ to 6.0. This differs from the theoretical expectation of the decrease of T_0 with the expansion of the universe. If the no-evolution behavior in this period is confirmed by future data, there must be other heating mechanisms to compensate the expansion cooling. One possible way is

through the reionization of He II. Current observation indicate that the reionization of He II ends at $z \simeq 3$ (e.g. Kriss et al. 2001; Theuns et al. 2002; Zheng et al. 2004). But it is unclear when the reionization of He II starts. If the reionization of He II is an extended process, say, starts from $z > 6$ and completes at $z \simeq 3$, it would be able to explain the no-evolution scenario of T_0 at $5 < z < 6$. This is also consistent with the fact that the predicted asymptotic thermal state (e.g., Hui & Haiman 2003) has never been reached at $z < 6$.

The explanation of extended He II reionization could be tested with the future observation of Cosmic Origins Spectrograph[1], which has enough sensitivity to probe the reionization history of He II. We point out that the Lyα leaks method of measuring the temperature of the IGM at $z \simeq 6$ should be applicable to He II Lyα leaks at $z \simeq 3$.

6.3. Summary

We show that the distribution of Lyα transmission fluxes and the profile of Lyα leaks are sensitive to the thermal state of the IGM at $z = 5$–6. This is due to the thermal broadening and the fact that only a few big leaks dominate the total flux. For lower temperature, there are more high peaks, and the profiles of leaks are narrower, while for higher temperature the profiles are smoother. Such features can be used to constrain the thermal state of the IGM.

The most sensitive statistic to the IGM temperature is the width function $n(W, z)$. We fitted the observed $n(W, z)$ of 7 quasars at $z \simeq 6$ to simulated $n(W, z)$ of different thermal states. The result shows that the allowed parameter space of (T_0, γ) is limited to a broad band and shows little evolution from $z = 5.1$ to 6.0. The most confident conclusion is that a low temperature of $T_0 < 1.3 \times 10^4$ K is difavored, which is also supported by the PDF of the flux. The result of no evolution from $z = 5.1$ to 6.0 implies that that the IGM should be heated by some mechanisms other than photoionization at $z \simeq 6$.

JRL thanks George Becker for answering questions on the reduction of raw spectra and ICRAnet for financial support. This work is supported in part by the US NSF under the grant AST-0507340. This research has made use of the Keck Observatory Archive (KOA), which is operated by the California Association for Research in Astronomy and the Michelson Science Center, under contract with the National Aeronautics and Space Administration.

[1] http://cos.gsfc.nasa.gov/

REFERENCES

Abel, T. & Haehnelt, M. G. 1999, ApJ, 520, L13

Becker, G. D., Sargent, W. L. W., Rauch, M., Simcoe, R. A. 2006, ApJ, 640, 69

Becker, G. D., Rauch, M. & Sargent, W. L. W. 2007, ApJ, 662, 72

Cen, R. & Ostriker, J. P. 1999, 514, 1

Ciardi, B., Stoehr, F. & White, S. D. M. 2003, MNRAS,343,1101

Fan, X. et al. 2006, AJ, 132, 117

Feng, L. L., Shu, C. W., & Zhang, M. P. 2004, ApJ, 612, 1

Feng, L. L., Bi, H. G., Liu, J. & Fang, L. Z. 2008, MNRAS in press, astro-ph/0710.5476

Gnedin, N. 2004 ApJ, 610, 9

Haehnelt, M. G. & Steinmetz, M. 1998, MNRAS, 298, L21

He, P., Feng, L. L., & Fang, L. Z. 2004, ApJ, 612, 14

He, P., Liu, J., Feng, L. L., Shu C. W. & Fang, L. Z. 2006, Phys. Rev. Lett, 69, 051302

Hui, L. & Gnedin, N. Y. 1997, MNRAS, 292, 27

Hui, L. & Haiman, Z. 2003, ApJ, 596, 9

Kelson, D. D. 2003, PASP, 115, 688

Kim, B., He, P., Pando, J., Feng, L. L. & Fang, L. Z. 2005, ApJ, 625, 599

Kriss, G. A., et al. 2001, Science, 293, 1112

Lidz, A., Oh, S. P. & Furlanetto, R. 2006, ApJ, 639, L47

Liu, J., Bi, H., Feng, L. L., & Fang, L. Z. 2006a, ApJ, 645, L1

Liu, J., Jamkhedkar, P., Zheng, W., Feng, L. L., & Fang, L. Z., 2006b, ApJ, 645, 861

Liu, J., Bi, H., & Fang, L. Z. 2007, ApJ, 671, L89

Liu, J. & Fang, L. Z. 2008, ApJ, 672, 11

Mellema, G., Iliev, I. T., Pen, U.-L., Shapiro, P. R. 2006, MNRAS, 372, 679

Miralda-Escude, J. & Rees, M. J. 1994, MNRAS, 266, 343

Qian, Y. Z. & Wasserburg, G. J. 2005, ApJ, 623, 17

Schaye, J., Theuns, T., Leonard, A., & Efstathiou, G. 1999, MNRAS, 310, 57

Seljak, U., & Zaldarriaga, M. 1996, ApJ, 469, 437

Sokasian, A, Abel, T., Hernquist, L, Springel, V. 2003, MNRAS, 344, 607S

Songaila, A. & Cowie, L. 2002, AJ, 123, 2183

Songaila, A. 2005, AJ, 130, 1996

Spergel, D. N. et al. 2007, ApJS, 170, 377

Stiavelli, M., Fall, S. M. & Panagia, N. 2004, ApJ, 610, L1

Theuns, T. et al. 2002, ApJ, 567, L103

Zaldarriaga, M., Hui, L., & Tegmark, M. 2001, ApJ, 557, 519

Zhang, T. J., Liu, J., Feng, L. L., He, P., & Fang, L. Z., 2006, ApJ, 642, 625

Zheng, W., et al., 2004, ApJ, 605, 631